



Nonlinear Variability Observed with Insight-HXMT in MAXI J1820+070 and MAXI J1535-571

Qi Ding^{1,2}, Long Ji³, Qing-Cui Bu⁴, Tiekuang Dong¹, and Jin Chang^{1,5}

¹ Key Laboratory of Dark Matter and Space Astronomy, Purple Mountain Observatory, Chinese Academy of Sciences, Nanjing 210033, China; tkdong@pmo.ac.cn

² School of Astronomy and Space Sciences, University of Science and Technology of China, Hefei 230026, China

³ School of Physics and Astronomy, Sun Yat-sen University, Zhuhai 519000, China; jilong@mail.sysu.edu.cn

⁴ Institut für Astronomie und Astrophysik, Kepler Center for Astro and Particle Physics, Eberhard Karls, Universität, Sand 1, D-72076 Tübingen, Germany

⁵ National Astronomical Observatories, Chinese Academy of Sciences, Beijing 100101, China
Received 2023 March 20; revised 2023 May 15; accepted 2023 June 2; published 2023 July 17

Abstract

We present the timing analysis of the nonlinear variability in two black hole low mass X-ray binaries MAXI J1820+070 and MAXI J1535-571 by using the bicoherence, a measure of phase coupling at different Fourier frequencies. We found different patterns, e.g., “cross” and “hypotenuse,” for LFQPOs in different outburst states. When they can be clearly distinguished, bicoherence patterns are similar over a wide energy range of 1–100 keV. It is intriguing that in some type-C QPOs we found the patterns that are normally observed in type-B QPOs. On the contrary, the “hypotenuse” pattern, a characteristic of type-C QPOs, was detected in a type-B QPO. This suggests that different types of QPOs may originate from similar underlying mechanisms. In addition, we speculate that the nonlinear variability may be a promising approach to disentangle distinct QPO models which assume different interactions between the broadband noise and QPO components.

Key words: black hole physics – instrumentation: detectors – methods: data analysis – X-rays: binaries

1. Introduction

A black hole low-mass X-ray binary (BH LMXB) is composed of a stellar mass BH and a late-type low-mass companion star. In some cases, it shows fast variabilities as relatively narrow peaks, known as quasi-periodic oscillations (QPOs), together with broadband noise in the Fourier power spectrum. QPOs in BH LMXBs can be divided into two categories according to their frequencies, i.e., low-frequency QPOs (LFQPOs; between a few mHz to 20 Hz) and high-frequency QPOs (HFQPOs; up to hundreds of Hz) (Motta et al. 2015). For LFQPOs, they can be further classified into three types, i.e., type-A, type-B and type-C QPOs (Wijnands et al. 1999; Casella et al. 2005). Among them, type-C QPOs are the most common, which have characteristic frequencies of 0.1 ~ 30 Hz with a high amplitude and usually appear in the hard or hard-intermediate states during outbursts. Type-B QPOs generally occur in the soft-intermediate state, which are believed to be associated with the jet. On the other hand, type-A QPOs, which manifest as wide and short peaks, are the least common and normally appear in the soft high state (for a detailed review, see Ingram & Motta 2019).

The origin of LFQPOs is under debate, although several theoretical models have been proposed by considering either the fluctuation of the accretion rate or the geometric precession of the accretion disk or the jet base (e.g., Tagger & Pellat 1999; Ingram & Done 2011; Stevens & Uttley 2016; Ma et al. 2021).

Additional methods offering a perspective beyond the traditional power spectrum are needed to investigate the formation mechanism of QPOs. Uttley et al. (2005) discovered the nonlinearity of broadband noise in accreting BH systems via a linear rms-flux relation and the lognormal distribution of the flux. Maccarone & Coppi (2002) suggest that the bicoherence, a measure of phase coupling at different Fourier frequencies, is a promising tool to study the high order variability. In general, there are three different patterns for observations showing type-C QPOs, i.e., “hypotenuse,” “cross” and “web” (Maccarone et al. 2011). The “hypotenuse” appears in a diagonal region where the two frequency components (f_1 and f_2) add up to the frequency of the QPO ($f_{\text{QPO}} = f_1 + f_2$), indicating the coupling of the QPO fundamental frequency and low-frequency broadband noise. For the “cross” pattern, the bicoherence shows up as frequency pairs where one frequency corresponds to f_{QPO} , and the other one can be any value. The “web” pattern is a combination of “hypotenuse” and “cross” types. On the other hand, the pattern of type-B QPOs is quite different, which appears as a high coherence region where both f_1 and f_2 are equal to f_{QPO} but no coupling is seen between QPOs and the broadband noise. The bicoherence has been studied in many sources, e.g., GRS 1915+105, XTE J1817-330 and H1743-322, indicating that it could be inclination-dependent and closely related to the different states during the evolution of outbursts in low mass X-ray binaries (Maccarone et al. 2011; Arur & Maccarone 2019, 2020, 2022). These

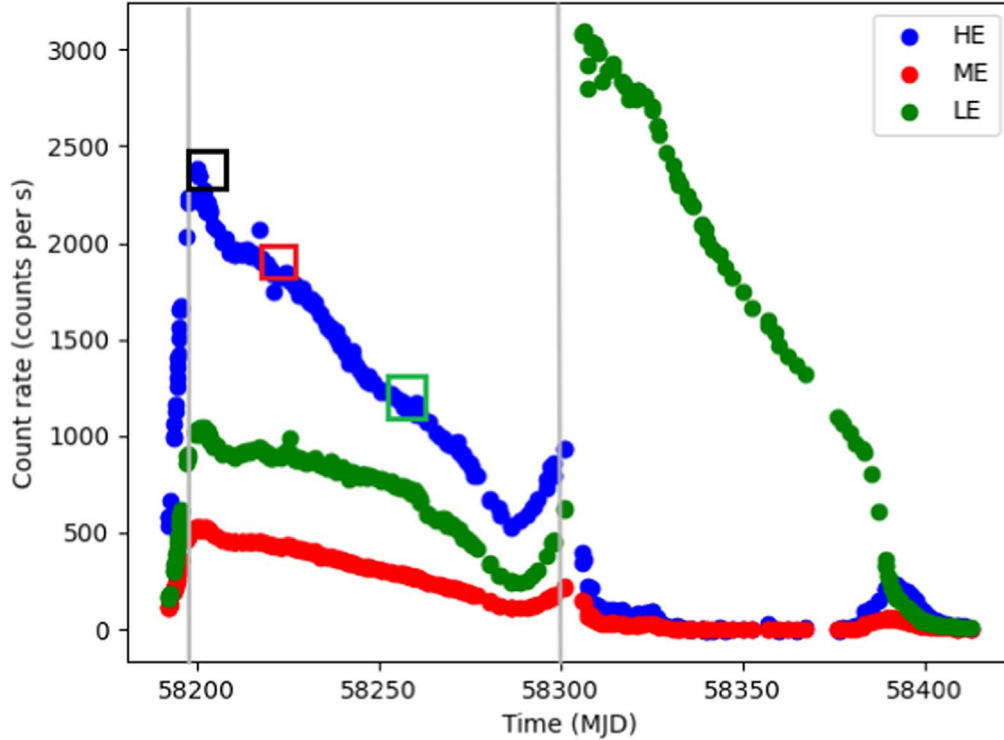


Figure 1. Long-term lightcurves of MAXI J1820+070 during its 2018 outburst observed with LE (1–10 keV; green), ME (10–30 keV; red) and HE (30–100 keV; blue) detectors. The period that presents QPOs is within two gray lines, i.e., MJD 58199–58300 (Ma et al. 2021). The observations that show clear bicoherence plots are marked in boxes, corresponding to the Obs-IDs P0114661003/P0114661004 (black), P0114661032 (red) and P0114661052 (cyan).

results are obtained by using the Rossi X-ray Timing Explorer (RXTE) that mainly has a large effective area below 30 keV. At higher energies, however, the bicoherence properties are still unknown.

In this study, we aim to investigate the broadband behavior of the bicoherence, especially extending to the hard X-ray energy band. We focus on the giant outbursts in MAXI J1820+070 and MAXI J1535-571, which are the brightest transients detected in recent years. Unprecedented data with ultra-high statistics and a wide energy range have been obtained by Insight-Hard X-ray Modulation Telescope (HXMT) observations. MAXI J1820+070 is a BH low mass X-ray binary discovered by Monitor of All-sky X-ray Image (MAXI) (Kawamuro et al. 2018). Its distance is 2.96 ± 0.33 kpc (Atri et al. 2020) and the mass of the central BH is $8.48^{+0.79}_{-0.72} M_{\odot}$ (Torres et al. 2020). Detailed temporal and spectral studies have been carried out by different authors (e.g., Kara et al. 2019; Ma et al. 2021; Zdziarski et al. 2021), indicating the presence of a vertically contracted corona or a precessed jet from which the QPOs are derived. MAXI J1535-571 is a transient discovered in 2017 (Negoro et al. 2017a) and then classified as a BH binary system based on the radio-X-ray luminosity relation and the rapid X-ray variability (Negoro et al. 2017b; Russell et al. 2019).

2. Observations and Data Analysis

Insight-HXMT, the first Chinese X-ray telescope, was successfully launched on 2017 June 15 (for details, see Zhang et al. 2020). It has a wide energy range and a large effective area, especially in the hard X-ray band, making it the best project for performing broadband timing studies. HXMT carries three main detectors, i.e., High Energy (HE) X-ray Telescope, Medium Energy (ME) X-ray Telescope and Low Energy (LE) X-ray Telescope. The HE telescope is composed of 18 cylindrical detection units, each of which is composed of a grating collimator and NaI (TI)/CsI (Na) composite crystals with a total geometric area of about 5100 cm^2 in the energy range of 20–250 keV (Liu et al. 2020). The ME telescope consists of 1728 independent Si-PIN detectors with a total effective area of 952 cm^2 in the energy range of 5–30 keV (Cao et al. 2020). The LE telescope contains a total of 96 Swept Charge Device (SCD) detectors with an effective area of 384 cm^2 in the energy range of 1–15 keV (Chen et al. 2020). In this study, we employed Insight-HXMT Data Analysis software (HXMTDAS) v2.05 and followed the official user’s guide⁶ for the data reduction. We selected events according to the following criteria: (1) the pointing offset angle $< 0^{\circ}04$; (2) the elevation angle $> 10^{\circ}$; (3)

⁶ <http://hxmtweb.ihep.ac.cn/SoftDoc/648.jhtml>

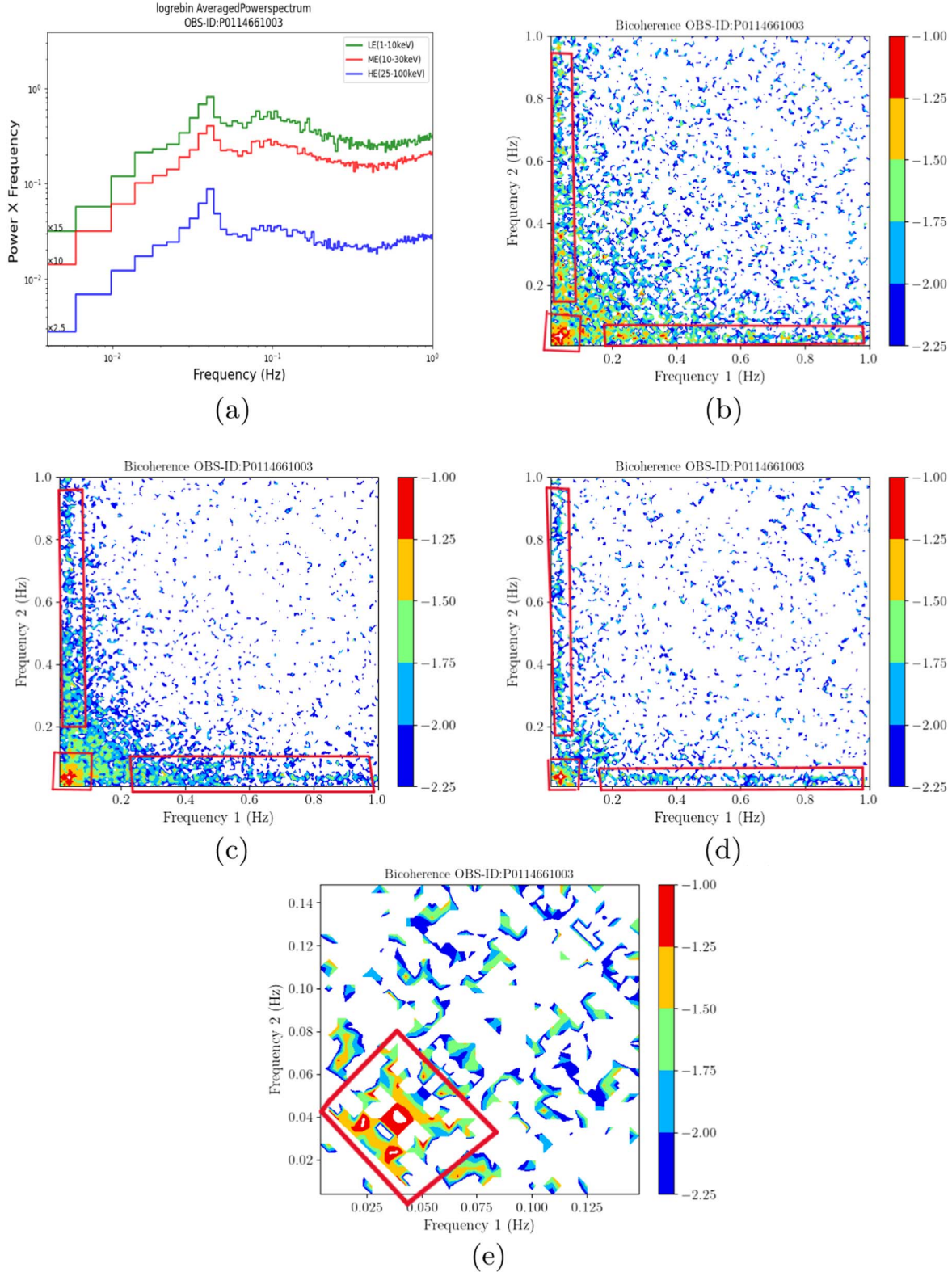


Figure 2. Panel (a): the power spectrum of MAXI J1820+070 for the Obs-ID P0114661003 observed with LE (1–10 keV; green), ME (10–30 keV; red) and HE (30–100 keV; blue) detectors, where narrow peaks around 0.4 Hz indicate QPOs. For clarity, we multiplied a constant factor for each power spectrum when plotting the figure. Panels (b), (c) and (d) present the bicoherence plots for LE, ME and HE respectively, where the “cross” pattern is clearly shown. Panel (e) shows a zoomed-in view of the HE band, making the high bicoherence region near $f_1 = f_2 = f_{QPO}$ clear. The highlighted vertical and horizontal features indicate the interaction between the high frequency noise and the QPO component. For clarity, high bicoherence regions are marked with red boxes. The color scheme of $\log b^2$ is as follows: dark blue:-2.0, light blue:-1.75, green:-1.5, orange:-1.25 and red:-1.0.

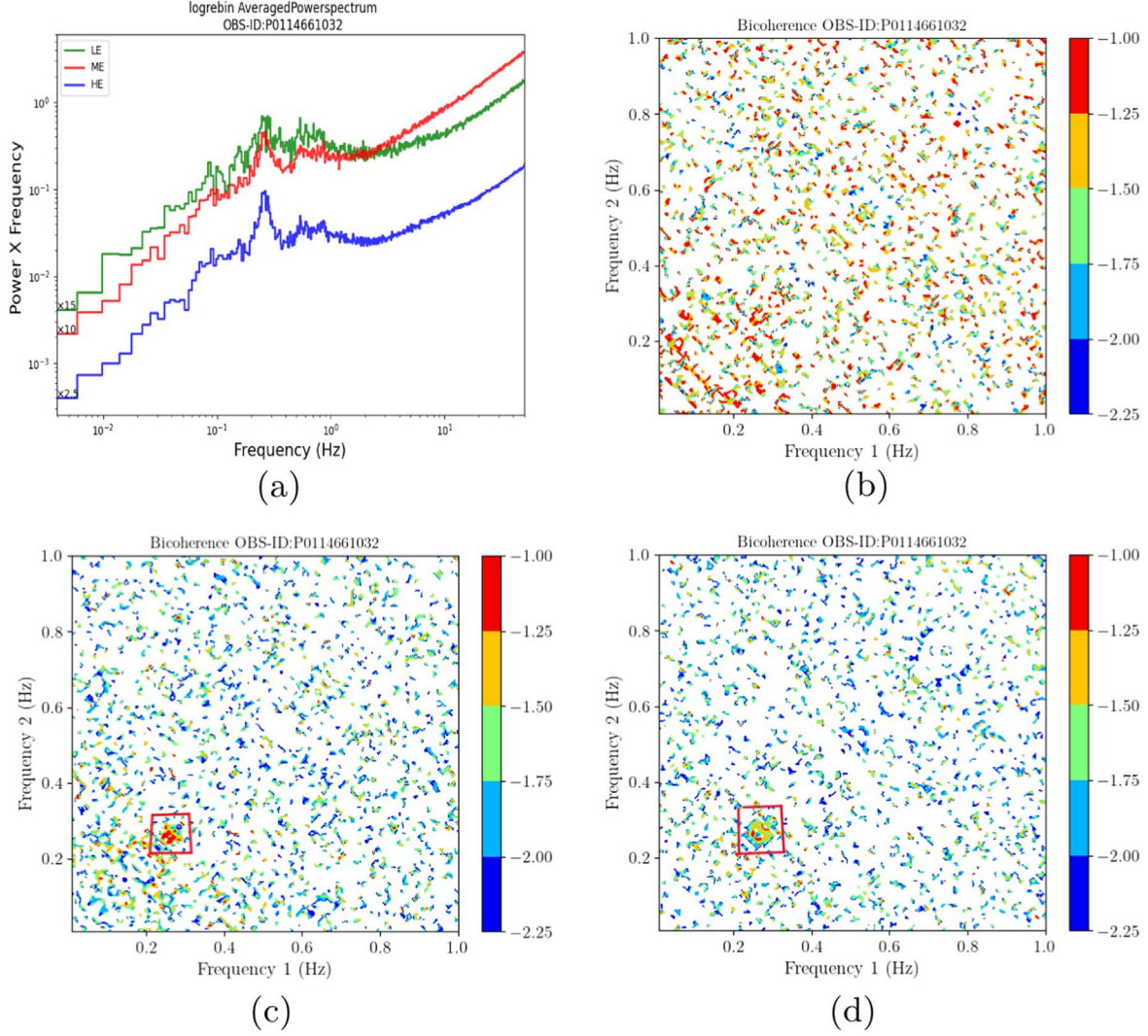


Figure 3. The same as Figure 2 but for the Obs-ID P0114661032. A high bicoherence region (marked with red boxes) appears around $f_1 = f_2 = f_{\text{QPO}}$ for ME and HE data.

the geomagnetic cutoff rigidity > 8 GeV. We only considered events within the small Fields-Of-View (FOVs).

The power spectra from MAXI J1820+070 and MAXI J1535-571 have been extensively studied by Ma et al. (2021) and Huang et al. (2018) respectively. Here we adopted their results and only considered the Insight-HXMT observations that present significant QPOs. In practice, the data set we used was between Modified Julian Date (MJD) 58192 and 58406 for MAXI J1820+070; and between MJD 58002 and 58177 for MAXI J1535-571. We extracted lightcurves in the energy ranges of 1–10 keV, 10–30 keV and 30–100 keV for LE, ME and HE data, respectively. Then, we divided the lightcurves into time intervals and calculated the bicoherence (b^2) using the normalization proposed by Kim & Powers (1979)

$$b^2(k, l) = \frac{|\sum X_i(k)X_i(l)X_i^*(k+l)|^2}{\sum |X_i(k)X_i(l)|^2 \sum |X_i(k+l)|^2},$$

where $X_i(k)$ is the result of the discrete Fourier transform of the i th time interval at the k th, l th and $(k+l)$ th frequencies⁷ and X_i^* is the complex conjugate of X_i . The lengths of time intervals we chose were 256 s for MAXI J1820+070 and 64 s for MAXI J1535-571 by considering QPOs' frequencies as reported by Ma et al. (2021) and Huang et al. (2018) respectively. The bicoherence has a value between 0 and 1, where 0 means no nonlinear coupling between the phases of different Fourier frequencies, and 1 suggests a complete coupling. The bicoherence has a non-zero mean even if there is no phase coupling between frequencies (Maccarone & Coppi 2002). Thus we subtracted a bias of $1/K$ from all bicoherence measurements, where K is the number of time intervals.

⁷ Note that the $(k+l)$ th frequency should be smaller than the Nyquist frequency.

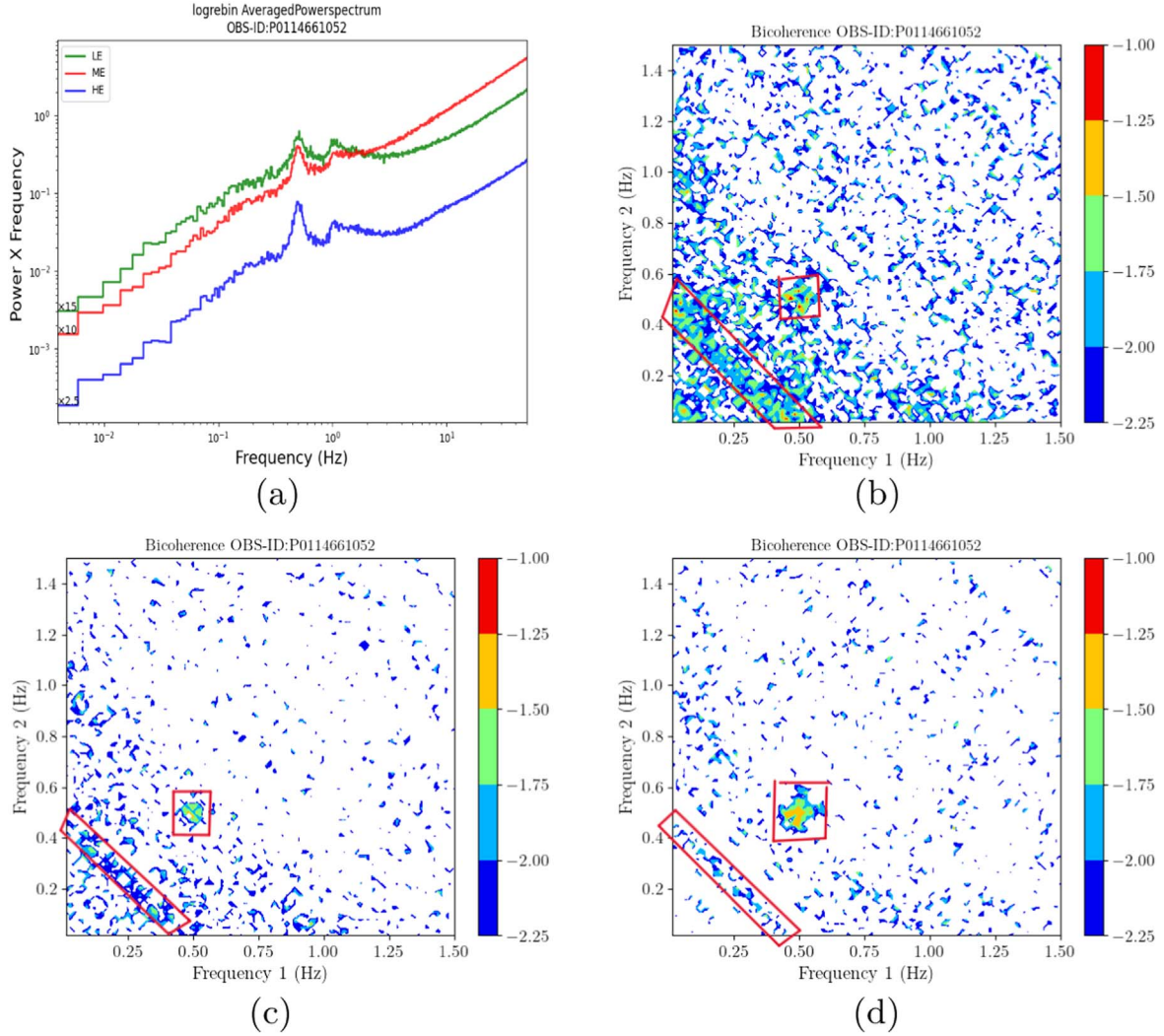


Figure 4. The same as Figure 2 but for the Obs-ID P0114661052. All LE, ME and HE data display the “hypotenuse” pattern, where the high bicoherence regions are highlighted with red boxes.

3. Results

3.1. MAXI J1820+070

Figure 1 plots the background-subtracted long-term light curves in energy ranges of 1–10 keV, 10–30 keV and 30–100 keV observed with LE, ME and HE detectors, respectively. It is clear that this source presents a canonical outburst evolution seen in low mass X-ray binaries, i.e., exhibiting the hard state, the hard intermediate state, the soft intermediate state and the soft state during MJD 58192–58400. We calculated the power spectrum of each observation by using the Python package STINGRAY (Huppenkothen et al. 2019). As an example, we display the result of the observational ID (Obs-ID) P0114661003 in the top left panel of Figure 2, where the prominent peaks indicate QPOs. We find that the centroid QPO frequency increases from 0.02 to

0.51 Hz, and then decreases to 0.22 Hz in the hard state of the outburst between MJD 58192 and 58300, which is consistent with the result of Ma et al. (2021).

We calculated the bicoherence for each observation and marked the observations that show representative and clear bicoherence plots in Figure 1, i.e., P0114661003/P0114661004, P0114661032 and P0114661052.⁸ For other observations, however, the pattern appears more vague or cannot even be firmly distinguished, probably because of the limited statistics although we cannot rule out the possibility of the variable phase coupling between frequencies. The bicoherence plots in the Obs-IDs P0114661003 and P0114661004 are similar, exhibiting a “cross” pattern, i.e., a

⁸ These four observations have an HE exposure time of at least 10^4 s, longer than most of the other observations.

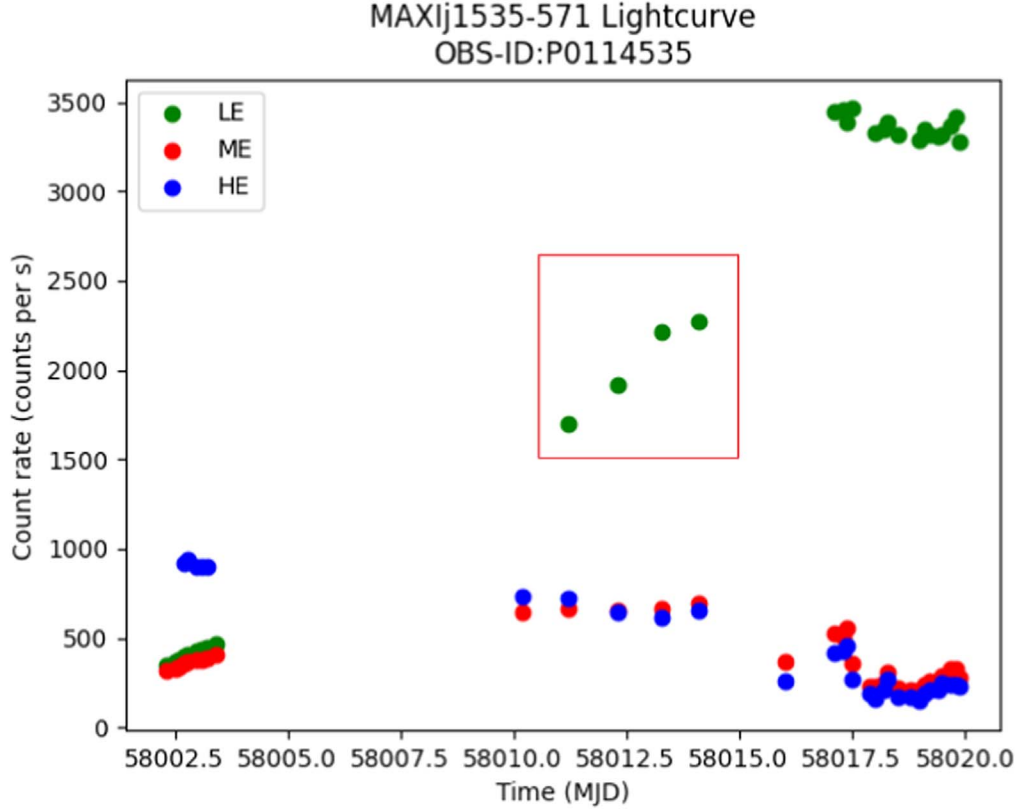


Figure 5. Long-term lightcurves of MAXI J1535-571 during its 2018 outburst observed with LE (1–10 keV, green), ME (10–30 keV, red) and HE (30–100 keV, blue) detectors. The observations exhibiting clear bicoherence patterns are highlighted in the red box.

high value where one frequency equals f_{QPO} and the other frequency can be of any value (Figure 2). This result is consistent with previous reports of hard states in other sources (e.g., Maccarone et al. 2011; Arur & Maccarone 2019, 2020, 2022). We note that no theoretical calculations of bicoherence plots are available so far, and therefore a quantitative comparison with theoretical models is out of the scope of this paper. We find that the bicoherence plots are quite similar for different energy bands, which suggests the underlying mechanism that dominates the coupling between QPO components and the broadband noise could be energy-independent. The bicoherence plots for the Obs-IDs P0114661032 and P0114661052 display different patterns. As shown in Figure 3, the former presents high bicoherence values only for the frequencies around $f_1 = f_2 = f_{\text{QPO}}$ in the energy bands of ME and HE.⁹ This pattern was only reported for type-B QPOs (e.g., Arur & Maccarone 2020), and instead the QPO in P0114661032 was classified as a type-C QPO (Ma et al. 2021). This implies a potential similarity between type-B and type-C QPOs, in particular regarding the interaction between the QPO formation region and the accretion flow.

⁹ For LE, the bicoherence pattern cannot be identified unambiguously.

On the other hand, the bicoherence plot for the Obs-ID P0114661052 exhibits a “hypotenuse” pattern (see Figure 4), i.e., high values for the diagonal region $f_1 + f_2 = f_{\text{QPO}}$ and the region around $f_1 = f_2 = f_{\text{QPO}}$, demonstrating a bicoherence evolution along with the outburst.

3.2. MAXI J1535-571

We show in Figure 5 the background-subtracted long-term lightcurves of MAXI J1535-571 in the energy ranges of 1–10 keV, 10–30 keV and 30–100 keV. QPOs that appear during the intermediate state of the outburst (red box in Figure 5) have been extensively studied by Huang et al. (2018) (for details, see Table 2 in their paper). We calculated the bicoherence plots for each observation and discovered visible patterns in Obs-IDs P011453500401/P011453500501 and P011453500701. Patterns that normally appear in type-B QPOs are shown in the HE band of the first two observations (Figure 6), although they were classified as type-C based on the features in the power spectra (Huang et al. 2018). On the other hand, at lower energies, their bicoherence plots do not present clear patterns. In contrast, patterns in the Obs-ID P011453500701 manifest an obvious “hypotenuse” shape

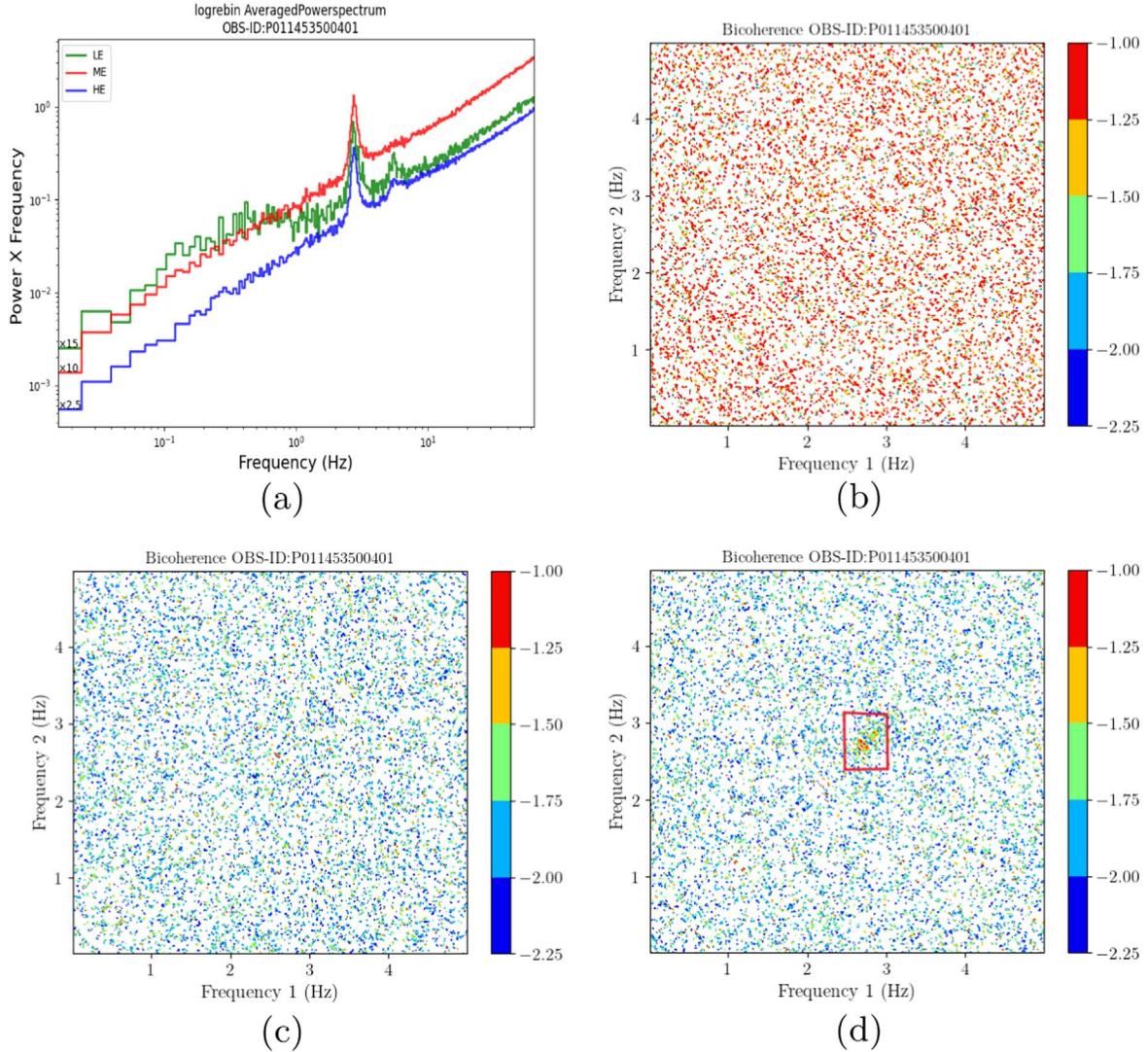


Figure 6. Panel (a): the power spectrum of MAXI J1535-571 for the Obs-ID P011453500401 observed with LE (1–10 keV; green), ME (10–30 keV; red) and HE (30–100 keV; blue) detectors. Panels (b), (c) and (d) present the bicoherence plots for LE, ME and HE respectively, where a high bicoherence region only appears at high energies around $f_1 = f_2 = f_{\text{QPO}}$ (marked with a red box). The color scheme is the same as in Figure 2.

(shown in Figure 7) which is normally observed in type-C QPOs, while it was considered as a type-B QPO by Huang et al. (2018).

4. Discussion

We studied the nonlinear temporal variability of two BH LMXBs (i.e., MAXI J1820+070 and MAXI J1535-571) during their outbursts observed with Insight-HXMT by using the bicoherence, a measure of phase coupling between different Fourier frequencies. In MAXI J1820+070, a “cross” pattern appears when the QPO frequency (f_{QPO}) is 0.045 Hz, and evolves into a “hypotenuse” pattern when $f_{\text{QPO}} = 0.23$ Hz. Changes of bicoherence patterns were reported in other sources

(e.g., GX 339-4) during transitions from a hard intermediate state to a soft intermediate state, and were proposed to be related to inclination angles of the sources (Arur & Maccarone 2020). They found that high inclination sources show a change from a “web” to a “cross” pattern, while low inclination sources present a change from a “web” to a “hypotenuse” pattern. In MAXI J1820+070, we discovered “cross” patterns when the f_{QPO} is low and “hypotenuse” patterns when f_{QPO} is relatively high, suggesting that it might be a low-inclination source, similar to GX 339-4 (see Figure 7 in Arur & Maccarone 2020). This seems to be consistent with the result ($\sim 30^\circ$) estimated by applying the reflection model (Bharali et al. 2019). However, we caution that most other estimations

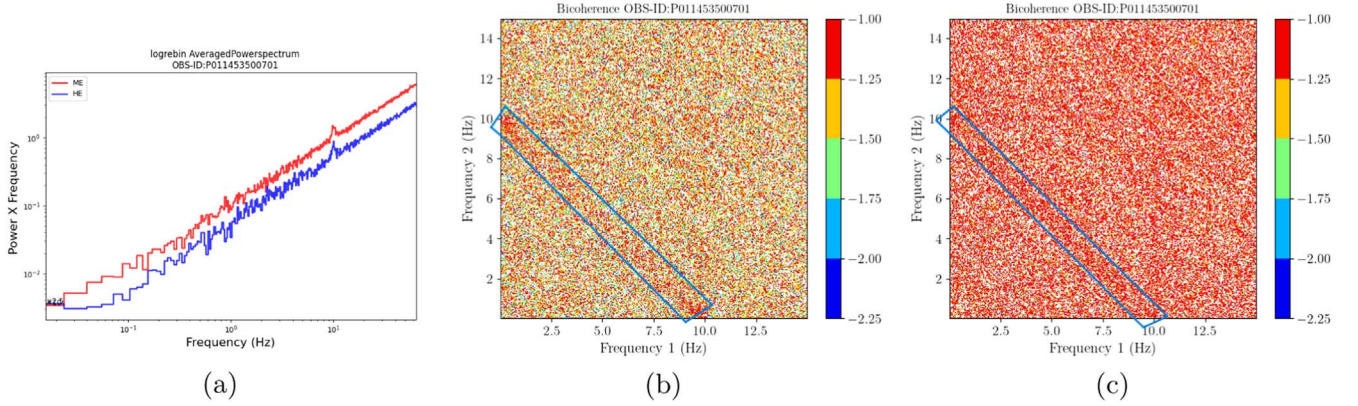


Figure 7. The same as Figure 6 but for the Obs-ID P011453500701. There are no available good time intervals for LE data. The bicoherence plots for ME (b) and HE (c) data show “hypotenuse” patterns, i.e., the high bicoherence regions at $f_1 + f_2 = f_{\text{QPO}}$ are marked with blue boxes.

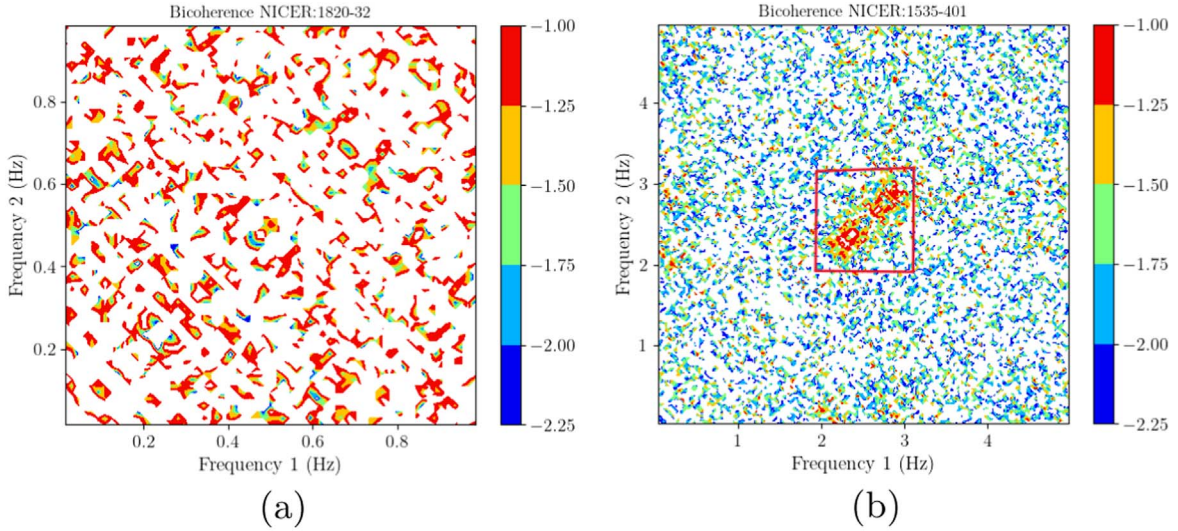


Figure 8. Bicoherence plots of NICER observations 1200120139 and 1050360108, which are nearly simultaneous with Insight-HXMT Obs-IDs P0114661032 (left) and P011453500401/501 (right). The high bicoherence region is marked with a red box.

suggest an inclination angle of $\sim 60^\circ$ based on the radio parallax, optical spectroscopy, the continuum-fitting method and proper motions of the ejecta (Atri et al. 2020; Torres et al. 2020; Wood et al. 2021; Zhao et al. 2021). Thanks to the wide energy coverage of Insight-HXMT, we investigated broadband bicoherence plots between 1 and 100 keV. We find that the patterns are quite similar in different energy bands, although in some cases they cannot be well recognized at low energies, i.e., Obs-ID P0114661032 for MAXI J1820+070 and Obs-ID P011453500401/501 for MAXI J1535–571. This is probably due to the small effective areas of LE and ME detectors. Alternatively, it could be also caused by the weak fractional variability at low energies because of the influence of thermal components (e.g., Kong et al. 2020; Ma et al. 2023). We tested these two possibilities by investigating nearly simultaneous

Neutron star Interior Composition Explorer (NICER) observations which have ultra-high statistics below 10 keV. The results are depicted in Figure 8, which only demonstrates a high bicoherence region around $f_1 = f_2 = f_{\text{QPO}}$ for Obs-ID P011453500401/501 in MAXI J1535–571, similar to the result of Insight-HXMT at high energies. On the other hand, for the NICER observation nearby Obs-ID P0114661032, no significant pattern is displayed. This implies that both of these two reasons can lead to low bicoherence values.

Based on previous studies, type-B and type-C QPOs exhibit different bicoherence patterns (Arur & Maccarone 2020). The main difference is that for type-C QPOs the high bicoherence regions are not only around $f_1 = f_2 = f_{\text{QPO}}$. However, in both MAXI J1820+070 and MAXI J1535–571 we find type-B-QPO-like patterns in type-C QPOs. In contrast, the type-B

QPO (Obs-ID P011453500701) found in MAXI J1535–571 presents a characteristic of type-C QPOs, i.e., “hypotenuse” patterns. This suggests that different types of QPOs may originate from similar underlying mechanisms. However, we cannot rule out the possibility that the statistics are not high enough to identify the “hypotenuse” and “cross” features even if they exist. This is partially supported by the fact that their patterns can be only seen in the HE band, where the count rate is highest (Figures 1, 5). In addition, the classification of QPOs might be potentially ambiguous, when the broadband noise can be fitted by either a power-law or a flat-top component in the power spectrum which is the primary criterion between type-B and type-C QPOs (Casella et al. 2005).

In theory, QPO models that produce a similar shape in power spectra might suggest different coupling between QPOs and the broadband noise components. For example, Zhou et al. (2022) proposed a new model in which the corona acts as a low-pass filter and the observed power spectrum is a result of the convolution between QPOs and the broadband noise, while their relation is additive in traditional models. This will result in a significant discrepancy in accounting for the lag spectrum and the explanation of the disk-jet precession model. We speculate that the bicoherence would be a promising diagnostic to disentangle between these QPO models and provide independent information on the accretion physics in BH LMXBs. Currently, no theoretical calculations have been carried out for the bicoherence of QPO models, which therefore are highly encouraged for quantitative comparisons with observations.

Acknowledgments

This work is supported by the National Natural Science Foundation of China (NSFC, grant Nos. 12173103 and U1738205). Tiekuang Dong is also supported by the China Scholarship Council under No. 202104910250. This work is based on observations with Insight-HXMT, a project funded by

the China National Space Administration (CNSA) and the Chinese Academy of Sciences (CAS).

References

- Arur, K., & Maccarone, T. J. 2019, *MNRAS*, 486, 3451
 Arur, K., & Maccarone, T. J. 2020, *MNRAS*, 491, 313
 Arur, K., & Maccarone, T. J. 2022, *MNRAS*, 514, 1720
 Atri, P., Miller-Jones, J. C. A., Bahramian, A., et al. 2020, *MNRAS*, 493, L81
 Bharali, P., Chauhan, J., & Boruah, K. 2019, *MNRAS*, 487, 5946
 Cao, X., Jiang, W., Meng, B., et al. 2020, *SCPMA*, 63, 249504
 Casella, P., Belloni, T., & Stella, L. 2005, *ApJ*, 629, 403
 Chen, Y., Cui, W., Li, W., et al. 2020, *SCPMA*, 63, 249505
 Huang, Y., Qu, J. L., Zhang, S. N., et al. 2018, *ApJ*, 866, 122
 Huppenkothen, D., Bachetti, M., Stevens, A. L., et al. 2019, *ApJ*, 881, 39
 Ingram, A., & Done, C. 2011, *MNRAS*, 415, 2323
 Ingram, A. R., & Motta, S. E. 2019, *NewAR*, 85, 101524
 Kara, E., Steiner, J. F., Fabian, A. C., et al. 2019, *Natur*, 565, 198
 Kawamuro, T., Negoro, H., Yoneyama, T., et al. 2018, *ATel*, 11399, 1
 Kim, Y. C., & Powers, E. J. 1979, *ITPS*, 7, 120
 Kong, L. D., Zhang, S., Chen, Y. P., et al. 2020, *JHEAp*, 25, 29
 Liu, C., Zhang, Y., Li, X., et al. 2020, *SCPMA*, 63, 249503
 Ma, X., Tao, L., Zhang, S.-N., et al. 2021, *NatAs*, 5, 94
 Ma, X., Zhang, L., Tao, L., et al. 2023, *ApJ*, 948, 116
 Maccarone, T. J., & Coppi, P. S. 2002, *MNRAS*, 336, 817
 Maccarone, T. J., Uttley, P., van der Klis, M., Wijnands, R. A. D., & Coppi, P. S. 2011, *MNRAS*, 413, 1819
 Motta, S. E., Casella, P., Henze, M., et al. 2015, *MNRAS*, 447, 2059
 Negoro, H., Ishikawa, M., Ueno, S., et al. 2017a, *ATel*, 10699, 1
 Negoro, H., Kawase, T., Sugizaki, M., et al. 2017b, *ATel*, 10708, 1
 Russell, T. D., Tetarenko, A. J., Miller-Jones, J. C. A., et al. 2019, *ApJ*, 883, 198
 Stevens, A. L., & Uttley, P. 2016, *MNRAS*, 460, 2796
 Tagger, M., & Pellat, R. 1999, *A&A*, 349, 1003
 Torres, M. A. P., Casares, J., Jiménez-Ibarra, F., et al. 2020, *ApJL*, 893, L37
 Uttley, P., McHardy, I. M., & Vaughan, S. 2005, *MNRAS*, 359, 345
 Wijnands, R., Homan, J., & van der Klis, M. 1999, *ApJL*, 526, L33
 Wood, C. M., Miller-Jones, J. C. A., Homan, J., et al. 2021, *MNRAS*, 505, 3393
 Zdziarski, A. A., Dzielak, M. A., De Marco, B., Szanecki, M., & Niedźwiecki, A. 2021, *ApJL*, 909, L9
 Zhang, S.-N., Li, T., Lu, F., et al. 2020, *SCPMA*, 63, 249502
 Zhao, X., Gou, L., Dong, Y., et al. 2021, *ApJ*, 916, 108
 Zhou, D.-K., Zhang, S.-N., Song, L.-M., et al. 2022, *MNRAS*, 515, 1914